Metabolic activity induces membrane phase separation in endoplasmic reticulum

Yihui Shen[a], Zhilun Zhao[a], Luyuan Zhang[a], Lingyan Shi[a], Sanjid Shahriar[b,c], Robin B. Chan[b,c], Gilbert Di Paolo[b,c], and Wei Min[a,d,1]

[a]Department of Chemistry, Columbia University, New York, NY 10027; [b]Department of Pathology and Cell Biology, Columbia University Medical Center, New York, NY 10032; [c]Taub Institute for Research on Alzheimer's Disease and the Aging Brain, Columbia University Medical Center, New York, NY 10032; and [d]Kavli Institute for Brain Science, Columbia University, New York, NY 10027

Membrane phase behavior has been well characterized in model membranes in vitro under thermodynamic equilibrium state. However, the widely observed differences between biological membranes and their in vitro counterparts are placing more emphasis on nonequilibrium factors, including influx and efflux of lipid molecules. The endoplasmic reticulum (ER) is the largest cellular membrane system and also the most metabolically active organelle responsible for lipid synthesis. However, how the nonequilibrium metabolic activity modulates ER membrane phase has not been investigated. Here, we studied the phase behavior of functional ER in the context of lipid metabolism. Utilizing advanced vibrational imaging technique, that is, stimulated Raman scattering microscopy, we discovered that metabolism of palmitate, a prevalent saturated fatty acid (SFA), could drive solid-like domain separation from the presumably uniformly fluidic ER membrane, a previously unknown phenomenon. The potential of various fatty acids to induce solid phase can be predicted by the transition temperatures of their major metabolites. Interplay between saturated and unsaturated fatty acids is also observed. Hence, our study sheds light on cellular membrane biophysics by underscoring the nonequilibrium metabolic status of living cell.

lipid metabolism | membrane phase | endoplasmic reticulum | Raman imaging | fatty acid

Lipid bilayers enclose the boundary of life, and their diverse chemical compositions together with physical phases underlie membrane organizations and biological functions (1). Studies of in vitro model membranes have shown that, depending on chemical composition, mixture of lipids in a bilayer could either blend into a uniform phase or phase-separate into coexisting domains due to immiscibility. Three major phases have been observed in these studies: liquid disordered (L_d), liquid ordered (L_o), and solid ordered (S_o), each representing a distinct type of bilayer organization (1, 2).

However, biological membranes are fundamentally different from in vitro model systems. As a manifestation, liquid phase separation gives rise to static microdomains that can be readily observed in model membrane, yet the existence of raft domains (L_o-like) in live cell has been a debate for decades due to much smaller domain size and faster dynamics (3). Many factors have been proposed to account for the unique aspects of biological membranes. One important factor is attributed to lipid–protein interaction, including the crowding effect of membrane protein as well as the intimate regulation by cytoskeleton (3, 4). Another less-considered but more fundamental factor concerns the thermodynamic state of the membrane. The living cell is an intrinsically nonequilibrium system that constantly undergoes lipid turnover and membrane trafficking. This is especially relevant and important for the endoplasmic reticulum (ER), the largest membrane system as well as the lipid metabolic center in cell. Indeed, the ER is subject to the influx of lipid molecules synthesized from fatty acids, the efflux due to vesicle budding and secretion, and the exchange of lipids with other organelles via

extensive and dynamic physical contacts (1). All of the above contribute to a fast turnover rate of ER lipids (half-life of ~100 h or one cell division) (5, 6).

With rich metabolic activity, ER membrane is easily perturbed from equilibrium by dynamic influx of nutrients. We hence hypothesize that the nonequilibrium factor, such as lipid synthesis in the ER, is capable of driving ER membrane from its poised L_d phase to phase separation. Our hypothesis is motivated by recent studies and findings. Experimentally, fatty acids such as palmitate have been reported to promote saturated lipid synthesis and accumulation in the ER, which subsequently impair ER structural integrity (7–9). However, the ER phase behavior was not examined there. Theoretical study has also alluded to local phase separation when patches of membrane with different composition are delivered to a bilayer (10). This could be relevant to the condition of active lipid synthesis occurring in the ER.

Toward testing this hypothesis, our study creates a nonequilibrium condition with the presence of lipid synthesis in ER membrane of living cells. To examine the spatial heterogeneity of membrane and interrogate its biophysical status, we employed the emerging vibrational imaging technique, that is, stimulated Raman scattering microscopy, and correlated it with lipidomics and fluorescence imaging. We found that ER membrane phase is susceptible to the modulation by metabolic activity. Remarkably, lipid synthesis derived from palmitate, a prevalent saturated fatty acid (SFA), even drives formation of solid-like domains, which

---

Significance

Membranes can adopt distinct phases. The endoplasmic reticulum (ER) is the largest membrane system inside cells and also harbors the richest metabolic activity including lipid synthesis. Unlike plasma membrane where separated "lipid raft" domains have been predicted and observed, ER membrane is thought to be uniformly fluidic. However, such understanding is based on biophysical studies of model membrane under thermodynamic equilibrium. It remains unclear whether and how lipid synthesis activity perturbs the equilibrium and promotes phase segregation in ER membrane. Herein, we utilized coherent Raman imaging technique to track lipid synthesis and surprisingly revealed solid-like domains emerging from liquid ER membrane. Interestingly, this phenomenon can be tuned by the incoming nutrient source, demonstrating the susceptibility of ER membrane to nonequilibrium modulation.

are rarely reported in live cells that presumably require fluidic membrane (4, 11–14). Interestingly, the propensity of phase separation can be tuned by the molecular identity of the metabolic flux: the ability of various fatty acids to induce solid-like domains is correlated with the transition temperatures of their major metabolites and might be related to their cytotoxicity. Our study surveys the ER phase behavior in the thermodynamic space of external perturbation and provides insight into membrane phase behavior of living cells far away from equilibrium.

Results

Palmitate Promotes Membrane Lipid Synthesis. The ER hosts the majority of de novo lipid synthesis in the cell (1). In this way, the ER is able to build new membrane components from external nutrients including fatty acids and supply the renewal of other membrane-bound organelles. In fact, it has been reported that palmitate, the most abundant fatty acid in circulation (15), promotes phospholipid synthesis and accumulation in the ER (7–9). To understand how palmitate metabolism reshapes the cellular lipidome and what types of lipid metabolites are accumulating, we analyzed changes in cellular lipid composition over time by HPLC-MS (Fig. 1 and Fig. S1).

The time-dependent lipid heat map (Fig. S1) reveals significant fold increase in glycerolipids [diacylglyceride (DG), triacylglyceride (TG), and phospholipids] and ceramide (Cer) ($P < 0.05$). This confirms that exogenous fatty acid promotes de novo lipid synthesis. Interestingly, when quantified by the change in absolute amount, several particular lipids show up in the highest rank of increase or decrease (Fig. 1). Besides TG, a common storage lipid, the major lipid accumulation is attributed to DG, phosphatidic acid (PA), phosphatidylinositol (PI), and phosphatidylcholine (PC) with two saturated fatty acyl chains (most likely 16:0 or 18:0). Meanwhile, there is a slight decrease in cholesterol ester (CE) and PC lipids with unsaturated acyl chains. In summary, palmitate caused time-dependent accumulation of fully saturated glycerolipids that elevated the overall lipid saturation in the cells.

Vibrational Imaging Reveals Dynamic Structures Derived from Lipid Synthesis. To examine the spatial heterogeneity of these newly synthesized lipids, we then sought to visualize their distribution and organization as well as relation to the ER in cells. Toward this, we employed the emerging vibrational imaging technique for stable-isotope–labeled small molecules (16). Specifically, the vibration of carbon–deuterium bond (C–D) in small molecules provides distinct chemical contrast for stimulated Raman scattering (SRS) microscopy (Fig. 2A). This platform is well-suited for studying lipid metabolism as well as membrane biophysics (16–19), since tagging small lipid molecules with relatively bulky
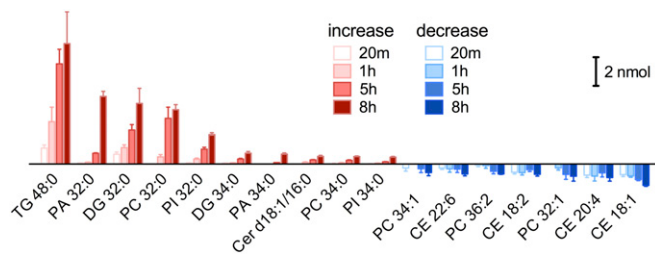
Fig. 1. Palmitate promotes synthesis and accumulation of saturated lipids. Alteration in major lipids after treatment by palmitate for 20 min, 1 h, 5 h, and 8 h. Change in amount between palmitate treated and control was calculated. Diagram shows top ranks in increase or decrease. CE, cholesterol ester; Cer, ceramide; DG, diacylglyceride; MG, monoacylglyceride; PA, phosphatidic acid; PC, phosphatidylcholine; PE, phosphatidylethanolamine; PI, phosphatidylinositol; PS, phosphatidylserine; SM, sphingomyeline; TG, triacylglyceride. Data are presented as mean ± SEM.
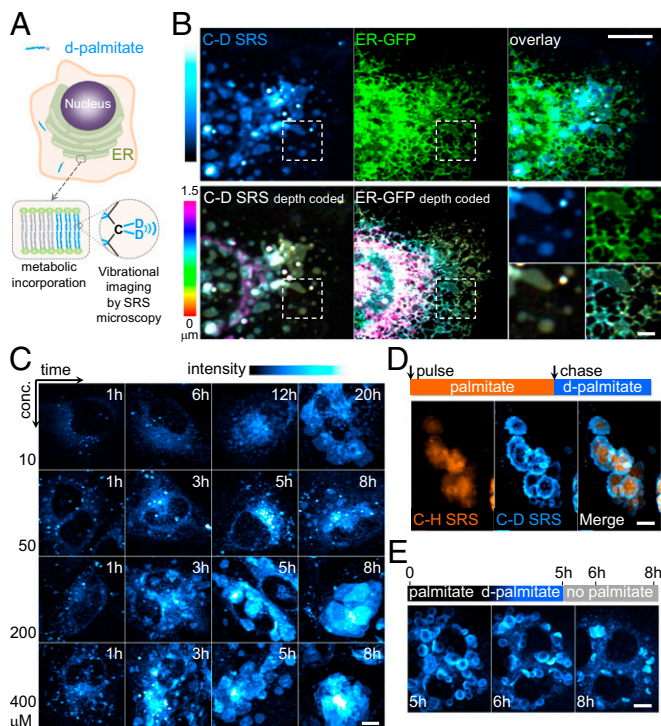
Fig. 2. Vibrational imaging reveals new dynamic structures formed by palmitate metabolites. (A) Illustration of isotope-SRS imaging: deuterium-labeled palmitate (d-palmitate) is metabolically incorporated into cellular lipids. The C–D bond vibration of the resulting metabolites is specifically detected by SRS microscopy. (B) ER-GFP–expressing HeLa cell was treated by 400 µM d-palmitate for 4 h. *Top* row shows 2D projection of ER-GFP fluorescence, C–D SRS, and their overlay. C–D SRS channel is pseudocolored cyan hot to show the full dynamic range of signal. *Bottom* row shows depth–color-coded image of ER-GFP and C–D SRS, and the magnified view of boxed regions. (C) C–D SRS images of HeLa cells treated with palmitate at varying dose (10~400 µM) and time (1~20 h). Four hundred micromolar fatty acid was used in this study, if not specified. (D) HeLa cells were pulse-chase treated with 4-h palmitate and 2-h d-palmitate, fixed, and washed by 0.5% Triton X-100. Two-color images are shown for C–H and C–D channels. (E) The clearance of palmitate-derived structures after removal of palmitate. HeLa cells were pulse-chase treated by 4-h palmitate and 1-h d-palmitate to better delineate the structures. Then palmitate was removed and C–D SRS image was taken at indicated time. (Scale bars: 10 µm; *Inset*, 2 µm.) Note: High-resolution images are available in the online full text version.

fluorophores often significantly perturbs lipid metabolism (20) (and will also be shown later in our study). Indeed, most common fluorescent tags such as NBD and BODIPY were termed "ill-suited" when used to study lipid biophysics (20, 21).

We treated cells with deuterium-labeled palmitate (d-palmitate) for several hours before acquiring C–D SRS images. We found that palmitate-derived lipids possessing the C–D label formed isolated micrometer-sized patches (Fig. 2B). We then correlated the C–D SRS image with confocal fluorescence from a luminal ER marker (ER-GFP) (Fig. 2B) or a membrane ER marker (mCherry-Sec61β) (Fig. S2 A and B) transiently expressed in the same cell, or from immune-stained ER membrane protein SERCA2 (Fig. S2 C and D). In this way, we confirmed that these new structures colocalized with the ER, consistent with ER accumulation of palmitate-derived lipids mentioned earlier (7).

Next, we studied the dynamics including both the growth and turnover of these structures. We supplemented HeLa cells with palmitate concentration varying from 10 to 400 µM for duration from 1 to 20 h (Fig. 2C). This is in reference to the free fatty acid concentration in circulation (fluctuating in a wide range from submillimolar to several millimolar) (22) and that commonly

applied in other studies [e.g., 400 μM (8, 23–25)]. We found that the new structures grew over time, faster at higher concentration (Fig. 2C). It appeared as isolated puncta in early stages and gradually developed into large lamellar structure. The development over time well correlates with the accumulation of palmitate metabolites revealed by lipidomics. Notably, these structures exist in a wide range of time and dose conditions we have used: at concentration down to 10 μM, or after as short as 1-h treatment (Fig. S3A). To resolve the growth dynamics in single cells, we performed a sequential treatment first by palmitate followed by d-palmitate. The later-applied label appeared on the rim, which suggests that the development of the structure is driven by accumulation of new palmitate metabolites at the periphery (Fig. 2D). These compartments disappeared gradually following removal of palmitate from the media, indicating that their development relies on the sustained influx of fatty acid (Fig. 2E). All of the above dynamic features suggest that these palmitate-derived structures were driven by cellular metabolic activity.

We further verified the above conclusion based on the following additional lines of evidence. First, although palmitate is reported to be toxic at high dose (26), no observable cell death occurred under the time and dose condition we used for imaging (Fig. S3B), which indicates that the cells are metabolically active. Second, quantification of intracellular free fatty acid (FFA) reveals a transient rise and then recovery to baseline level within 3 h (Fig. S3C). Thus, FFA alone is not sufficient to form such stable structures over a long time. Last, these structures were abolished by small-molecule inhibitor of acyl-CoA synthetase that catalyzes the first step in lipid synthesis (27) (Fig. S3 D and E), and were also suppressed by siRNA of GPAT4, an enzyme involved in phospholipid synthesis (28) (Fig. S3 F and G).

Newly Synthesized Lipids Form Phase-Separated Membrane Domains in the ER. Given the observed dynamic accumulation of palmitate metabolites in ER, we asked whether ER membrane phase had been affected. To test this, we first examined if the new structures are membrane, and then evaluated if they are phase-separated domains from the fluidic ER.

We confirmed that they were not lipid droplets (LDs) where neutral lipid metabolites (TAG and CE) are stored using Nile Red staining. At early stage (1-h incubation), LDs as stained by Nile Red already accumulate significant C–D signal that appear saturated in intensity (Fig. 3A, arrows). Meanwhile, the majority of palmitate-derived structures lacked staining by Nile Red. Intensity profiles imply that the failure of staining in the latter structure is not due to poor Nile Red contrast in small nascent LDs (Fig. 3A). We further confirmed they did not correlate with nascent LD sensor cherry-LiveDrop (29) (Fig. S4A). In fact, quantitative image analysis of the Nile-Red–positive and –negative structures reveals significant difference. LDs can be easily distinguished in the image as small intense puncta. However, the non-LD structures exhibit wider distribution in size but weaker and more uniform intensity than LDs (Fig. S4 B and C), suggesting a lamellar organization. Indeed, morphologically, reconstructed z-stack images revealed planar micrometer-sized structures in x–y but with diffraction-limited z profiles (Fig. 3B). This fits into the model where planar membrane bilayer lies parallel to the illumination plane (Fig. 3C). In cells where individual compartments are no longer resolvable from each other, we could always find step-like features in the line profile of C–D SRS intensity (Fig. 3D). We could then identify an equal spacing after calculating pairwise intensity difference (Fig. 3E) (14 ± 5 μV in HeLa and 19 ± 6 μV in COS-7). As an estimation, this intensity spacing translates into 3.1×10^6 palmitoyl groups in focus, which approximates to the SRS signal size calculated from one deuterated lipid bilayer, suggesting the compositional unit to be lipid bilayer (*Supporting Information*). Thus, in parallel with lipidomic analysis that the accumulating lipids (DG, PA, PI, and PC) are all membrane constituents (Fig. 1), these pieces of evidence
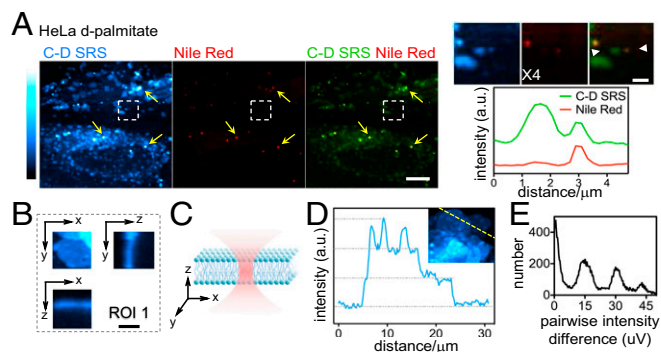
Fig. 3. Image quantification and analysis reveals membrane features of palmitate-derived structure. (A) C–D SRS, Nile Red fluorescence, and overlay images of HeLa cell treated with d-palmitate for 1 h and stained by Nile Red. Yellow arrows indicate LDs stained by Nile Red. On the *Right*, magnified images are shown for the boxed area. Intensity line profiles are plotted for both channels between the white triangles. (B) HeLa cell was treated with d-palmitate for 5 h. Orthogonal views of a representative non-LD palmitate-derived structure from depth-resolved reconstructed image are shown. (C) Cartoon showing a planar bilayer illuminated in laser focus. (D) Line profiles of C–D SRS image with overlapping layers of palmitate metabolites. (E) Pairwise distribution function was calculated for these line profiles, which show oscillating patterns that indicate constant intensity spacing. (Scale bars: major, 10 μm; *Inset*, 2 μm.)

from imaging strongly support that palmitate-derived lipids are forming membrane.

In fact, forming domains instead of blending into existing ER membrane already implies different organization in palmitate-derived lipids from the native ER membrane. We then further examined the spatial relation of these domains to ER membrane using two types of membrane markers, one lipid (BODIPY-C$_{12}$) and one membrane protein (mCherry-sec61β). BODIPY-C$_{12}$ is a common fluorescent analog of palmitate (Fig. 4A) and also serves as a general membrane lipid marker. Thus, we added trace BODIPY-C$_{12}$ along with d-palmitate. Remarkably, different patterns were observed in the correlative SRS and fluorescence images (Fig. 4B). While C–D SRS exhibited many isolated domains, BODIPY-C$_{12}$ highlighted reticular structure resembling the ER. Even negative correlation can be observed between BODIPY fluorescence and C–D SRS channel in flat regions of ER membrane such as large sheet and nuclear envelope (Fig. 4C and Fig. S5 A–C). This observation, on one hand, could be reconciled by strong perturbation from the BODIPY tag. On the other hand, it supported the hypothesized lateral phase separation in ER membrane, since bulky fluorescent probes usually favor partitioning into disordered over ordered phase in vitro (20).

This lateral phase separation can be further verified with an ER membrane protein marker, mCherry-Sec61β (Fig. 4D). Specifically, on large sheets, negative correlation can be clearly identified between C–D SRS and mCherry fluorescence channels (Fig. 4E). Special considerations must be taken when examining the lateral heterogeneity in ER membrane. Different from plasma membrane or vesicle, the ER has a unique architecture composed by tubular and lamellar cisternae. We noted that the planar structure of C–D SRS domains fits into the model of so-called "ER sheet" (lamellar cisternae), where a lamellar space is enclosed by two opposing membrane bilayers. Palmitate metabolites completely occupied one layer (and expand ER sheet), while forming intercalating domains on fluidic ER on the other layer (Fig. S5D). This is manifested in the line profiles of C–D SRS that negatively correlates with fluorescence channel (Fig. 4 C and E and Fig. S5C).
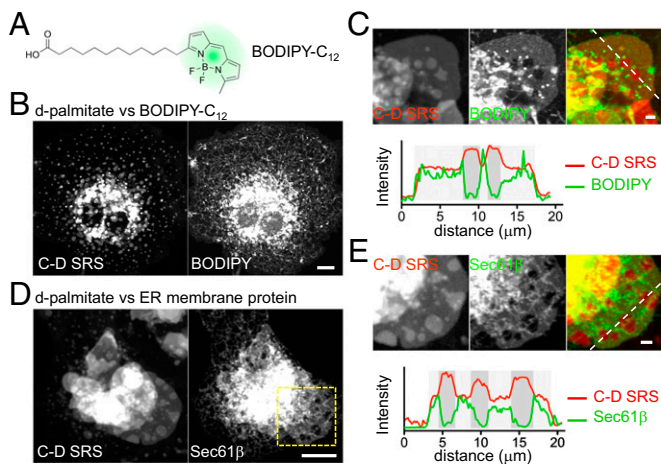
Fig. 4. Fluorescent membrane markers reveal lateral separation of palmitate-derived membrane domains in the ER. (*A*) Chemical structure of fluorescent analog, BODIPY-C$_{12}$. (*B*) COS-7 cell was treated with d-palmitate and 2 μM BODIPY-C$_{12}$ for 5 h. C–D SRS and BODIPY fluorescence are shown. (*C*) Magnified view is shown for a large sheet. Intensity profiles of the dashed line are shown for both SRS (red) and fluorescence (green) channels. (*D*) mCherry-Sec61β–expressing COS-7 cell was treated with d-palmitate for 4 h. C–D SRS and Sec61β fluorescence are shown. (*E*) Magnified view is shown for the boxed area in *D*. Intensity profiles of both SRS (red) and fluorescence (green) channels are shown for the dashed line in *D*. In *C* and *E*, dark gray stripes indicate two layers of palmitate-derived membrane. (Scale bars: major, 10 μm; *Inset*, 2 μm.) Note: High-resolution images are available in the online full text version.

Emergence of Solid-Like Domain in ER Membrane. Unlike plasma membrane (about 50% cholesterol), ER membrane is characterized by low cholesterol level [3–6% of lipids (30)]. This predicts unique phase behavior in ER membrane, because cholesterol is known to eliminate solid–liquid transition and promote L$_o$-phase formation in in vitro model membrane (31). Accordingly, ER membrane in its normal state is believed to adopt uniform L$_d$ phase due to low lipid saturation (1, 14, 32), but meanwhile is potentiated for L–S$_o$ phase separation if saturation level elevates sufficiently (Fig. S6). Since palmitate-induced lipid synthesis introduces into the ER new membrane components that are overall more saturated, we hypothesized that such influx was able to drive solid-like domain separation from the otherwise L$_d$-like ER. Solid phase is characterized by highly ordered acyl chain packing, as well as ultraslow lateral motion (Fig. S6). Thus, to test our hypothesis, we first evaluated the conformational order and then estimated the translational mobility of lipids within these domains.

In Raman spectroscopy, acyl chain conformational order could be inferred from the Raman peak width of CD$_2$ symmetric stretch vibration at 2,101 cm^{-1}: the more ordered, the narrower the peak (33). The Raman spectra measured from d-palmitate–treated cells (Fig. 5*A*, cell 25 °C or 37 °C) resembled that from d$_{62}$-DPPC in the ordered (presumably S$_o$) phase (Fig. 5*A*, d$_{62}$-DPPC 25 °C), but displayed pronouncedly narrower peaks than d$_{62}$-DPPC or d$_{31}$-POPC in L$_d$ phase (Fig. 5*A*, d$_{62}$-DPPC 42 °C and d$_{31}$-POPC 25 °C). To offer more spatial information, we performed ratiometric SRS imaging between 2,101 and 2,168 cm^{-1} to map the conformational order of intracellular palmitate metabolites. Consistently, with reasonable heterogeneity, the membrane domains display high 2,101/2,168 cm^{-1} ratio close to the ordered phase (Fig. 5*B*). Hence, in situ Raman microspectroscopy and SRS spectral imaging unraveled a marked increase in acyl chain conformational order on the palmitate-derived membrane domains.

We then sought to evaluate the translational mobility within the phase-separated domains. Since fluorescent probes failed to incorporate into these domains (Fig. 4), we relied on pulse-chase SRS imaging to estimate the lateral diffusion coefficient (*D*). We

sequentially treated the cells with d-palmitate, then regular palmitate, and finally d-palmitate again, and observed a bull's-eye-like pattern in the C–D SRS channel (Fig. 5*C*). Similar bull's-eye pattern was observed for a longer-chain SFA, stearic acid (Fig. 5*D*). By estimation, if these domains were in the liquid phase, one would predict homogeneous C–D signal distribution within individual domains (2D free diffusion displacement $d = 5{\sim}10$ μm) due to fast lateral diffusion [$D(L_d) \sim 1$ μm^2/s, $D(L_o) \sim 10^{-1}$ μm^2/s] (1, 34). Semiquantitatively, Gaussian fitting of the line profiles yielded an estimated *D* about 10^{-4} μm^2/s (*Supporting Information*), which is close to that in S$_o$ phase [$D(S_o) \sim 10^{-3}$ μm^2/s (1, 34)]. Moreover, collision between separate domains was also captured (Fig. 5*E*). Interestingly, the collided domains neither completely fuse nor recover the circular morphology in nearly half an hour, again suggesting that they are in solid phase wherein intradomain interaction overcomes line tension. Therefore, with various
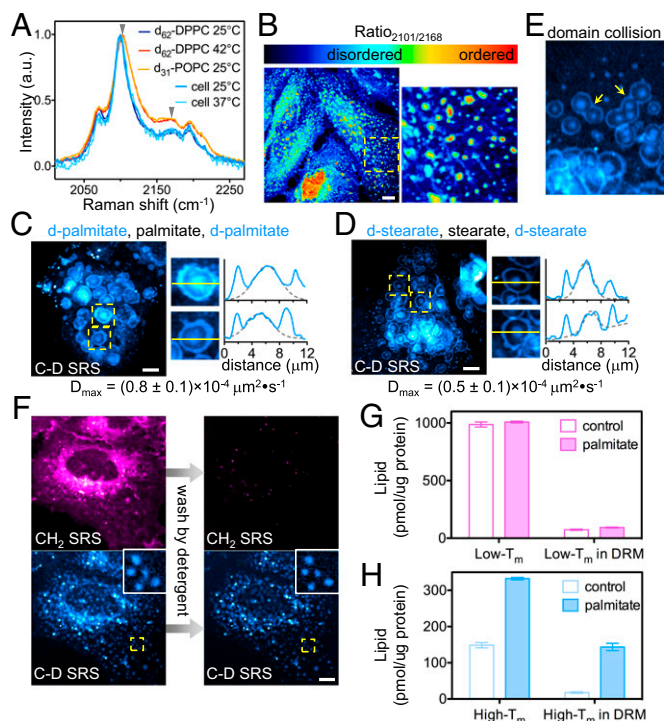
Fig. 5. Palmitate-derived membrane domains exhibit solid-like properties as high conformational order and low translational mobility. (*A*) Normalized Raman spectra of d$_{62}$-DPPC dispersion (at 25 and 42 °C) and d$_{31}$-POPC dispersion (at 25 °C) overlaid with Raman spectra of HeLa cells treated with d-palmitate for 5 h (acquired at 25 and 37 °C). Arrowheads mark peak (2,101 cm^{-1}) and shoulder (2,168 cm^{-1}) frequencies used for spectral imaging in *B*. (*B*) Calculated C–D SRS ratiometric image of 2,101/2,168 cm^{-1} for HeLa cells treated with d-palmitate for 3 h. Magnified images are shown on the *Right*. (*C*) C–D SRS images of HeLa cell sequentially treated with d-palmitate (3 h), palmitate (1.5 h), and d-palmitate (0.5 h). Intensity profiles (blue) were measured across the yellow lines in regions of interest and fitted with Gaussian function (gray dashed). The estimated maximum diffusion coefficient (D_{max}) is shown below (mean ± SEM; *n* = 13). (*D*) Similar to the sequential treatment in *C*, d-stearate (1 h), stearate (1.5 h), and d-stearate (0.5 h) were used instead of palmitate. D_{max} is shown below (mean ± SEM; *n* = 21). (*E*) Domain collision (arrows) captured in cells treated as in *C*. (*F*) HeLa cell was treated with d-palmitate for 1 h. CH$_2$ and C–D SRS images were taken before (*Left* column) and after (*Right* column) being washed by 0.5% Triton X-100 for 10 min at 4 °C. (*G* and *H*) Changes in low-T$_m$ (*G*) and high-T$_m$ (*H*) lipid concentration in total lipid extract or detergent-resistant lipid fraction (DRM) after palmitate treatment for 5 h. Major species DG, PA, PI, PC, PE, and PS are included in quantification. Data are presented as mean ± SD. (Scale bars: 10 μm.)

characterizations, we confirmed the existence of solid-phase membrane in living mammalian cells.

High-T_m Palmitate Metabolites Provide Driving Force for Phase Separation. To gain insight into the molecular driving force underlying solid-like domain, we evaluated the phase transition temperature (T_m) of accumulated lipids highlighted in lipidomics (Fig. 1). We noted that those 32:0 and 34:0 lipids all bear significantly higher T_m (T_m = 41~67 °C, Table S1) than physiological temperature, which could account for the driving force of L–S$_o$ phase separation under the low cholesterol presented in the ER (Fig. S6).

To further test whether high-T_m lipids are indeed enriched in phase-separated membrane domains, we performed detergent wash by Triton X-100 following palmitate treatment (4). Resistance to nonionic detergent such as Triton X-100 at 4 °C is a classical assay used to identify the existence of potentially ordered membrane domain. SRS imaging revealed that C–D domains but not the majority of endogenous CH$_2$-bearing lipids showed resistance to detergent wash (Fig. 5F). We then did parallel lipidomic analysis on control or palmitate-treated cells before and after detergent wash (Fig. S7 A and B). We divided the major lipid species (DG, PA, PI, and PC) into high-T_m (T_m > 37 °C) and low-T_m (T_m < 37 °C) categories and quantified each category in total lipid extract or detergent-resistant fraction (Fig. 5 G and H). First, the result shows that new lipid synthesis is dedicated to high-T_m lipids but not low-T_m lipids; thus, increase in high-T_m lipids is well correlated with appearance of C–D SRS signal. Second, the increased portion of high-T_m lipids is mostly retained after detergent wash while low-T_m lipids are not. This further pinpointed the direct involvement of high-T_m lipids in the formation of detergent-resistant C–D SRS domains. Similar detergent-resistant membrane pattern was also observed following treatment of regular palmitate, which rules out the possible interference of isotope labeling (Fig. S7 C and D). Therefore, the lipidomic and imaging analysis together demonstrate the preferred localization of high-T_m lipids within solid-like membrane domains, supporting that high-T_m metabolites were indeed the molecular driving force for such phase separation.

ER Membrane Phase Separation Can Be Tuned by Fatty Acid Unsaturation and Chain Length. Based on the hypothesized connection between high-T_m lipids and membrane domain formation, ER phase separation should be dependent on the molecular identity of the fatty acid and can be predicted by the T_m of its main lipid metabolites. Thus, we similarly applied a common unsaturated fatty acid (UFA), oleate, whose metabolites (e.g., DOPC) possess very low T_m due to the unsaturation in the acyl chain (Table S1). The colocalization of C–D SRS to Nile Red fluorescence reveals that oleate is incorporated almost exclusively into LDs, and did not form membrane domains (Fig. 6A).

We went on to test a set of deuterated SFAs including lauric acid (C12:0), myristic acid (C14:0), palmitic acid (C16:0), and stearic acid (C18:0). Their metabolites show elevating T_m values due to increasing fatty acyl chain lengths (Table S1). In agreement with our hypothesis, they exhibited increasing capability to drive large-scale phase separation at the same concentration (Fig. 6B): C12:0 does not form visible membrane domains but numerous LDs even after prolonged treatment; C14:0 only forms domains with limited size (~1 µm); C18:0 forms large-scale membrane structures even faster than C16:0 does.

Notably, in the functional sense, we found similar dependence for fatty-acid–induced cell death (Fig. 6C). Cell death was observed only after prolonged incubation with the long-chain SFA C16:0 and C18:0, but not with UFA or short-chain SFA. This dependence is also correlated with stress markers reported elsewhere that are mutually independent, including Akt/protein kinase B (Akt/PKB) signaling, activation of Jun N-terminal kinase (JNK), and the unfolded protein response (UPR) (25, 35). Thus,
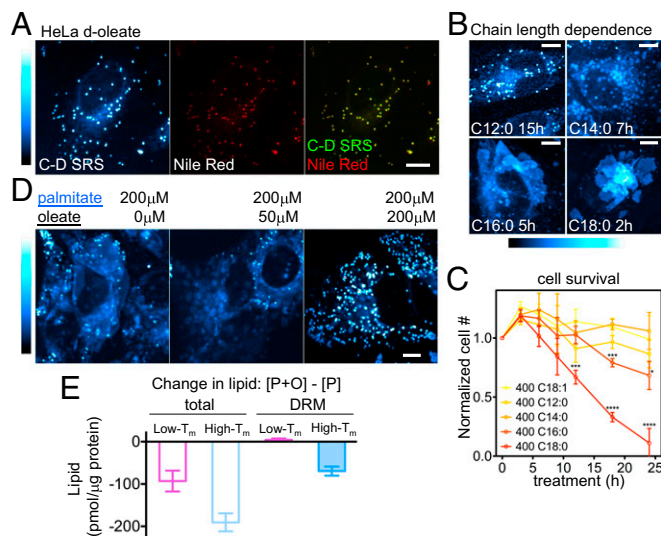
Fig. 6. The tendency to form solid-like membrane can be tuned by fatty acid identity and combination. (A) C–D SRS, Nile Red fluorescence, and overlay images of HeLa cell treated with d-oleate for 1 h and stained by Nile Red. (B) C–D SRS images of HeLa cells treated with C12:0 (15 h), C14:0 (7 h), C16:0 (5 h), and C18:0 (2 h). (C) Normalized cell number after treatment of designated fatty acid and duration. Data are presented as mean ± SEM; n = 4. *P < 0.05; ***P < 0.005; ****P < 0.001. (D) C–D SRS images of HeLa cells treated with combination of d-palmitate and increasing concentrations of oleate. (E) Changes in low-T_m and high-T_m lipid concentration in cells cotreated by 400 µM palmitate and 200 µM oleate (P + O) compared with 400 µM palmitate alone (P). Data are presented as the amount difference between "P + O" and "P" ([P + O] − [P]) in total lipid extract (total) and detergent-resistant fraction (DRM). (Scale bars: 10 µm.)

the metabolic effect of a fatty acid might be predicted by simple physicochemical principle regarding the T_m of its metabolites.

Interplay Between Fatty Acids in Modulating ER Membrane Phase Separation. Since the plasma consists of a complex and fluctuating mixture of SFA and UFA (15), this further raises an interesting question whether fatty acids could influence each other in the metabolic modulation of ER membrane phase. Noticing the relatively low T_m of POPC, we hypothesized that oleate might prevent the system from being driven by palmitate to phase separation.

Thus, we added oleate together with d-palmitate to study its influence on the phase separation potential of the latter (Fig. 6D). Biochemical studies have found that oleate can channel palmitate into LDs (23), which is also manifested in C–D SRS images from our experiment. However, more importantly, oleate also diminished the solid-like domains in a concentration-dependent manner. Note that, in this context, oleate itself stays excluded from the remaining solid-phase membrane (Fig. S8 A and B). Oleate was also able to reduce solid membrane after its formation in a pulse-chase manner (Fig. S8C). Similar to oleate, docosahexaenoic acid (DHA) (22:6), a polyunsaturated fatty acid, was also able to reduce the area of palmitate-derived solid membrane domains (Fig. S8D).

In parallel, we compared the lipid profile after cotreatment of oleate to that only treated by palmitate. Both total lipid extract and detergent-resistant fraction show significant alteration by oleate. The effect of oleate is clearly reflected in the level of low-T_m and high-T_m lipids (Fig. 6E). In total lipid extract, oleate reduced more high-T_m lipids than low-T_m lipids. In detergent-resistant fraction, which is more specific to the solid-phase membrane, oleate also significantly reduced high-T_m lipids but did not affect low-T_m lipids. Therefore, in supplementation to the current understanding that accumulation of neutral lipids is

cytoprotective, a previously unknown mechanism for UFA to rescue the cytotoxicity of SFA might lie in its ability to destruct the solid-like membrane.

Discussion

By taking advantage of live-cell SRS microscopy coupled with minimally perturbative isotope labeling, we discovered that the influx of high-T_m lipids caused by SFA metabolism could drive the formation of large-scale membrane domains in the ER. Remarkably, the newly formed domains exhibited solid-like characteristics as detergent resistance, high conformational order, ultraslow lateral diffusion, strong intradomain interaction, and large-scale structural stability. Our observation thus reveals the susceptibility of ER membrane phase to the metabolic activity, and, to some extent, corroborates the theoretical prediction under non-equilibrium condition (10). Here, we want to emphasize that the earlier work by Fan et al. (10) focuses on L_o–L_d phase separation to account for lipid raft on plasma membrane, and the non-equilibrium condition there largely refers to vesicle delivery. The biological manifestations are different here for the ER with all of the unique characteristics such as low cholesterol level and high de novo lipid synthesis activity, although the conclusion drawn from our study converges to a similar physical principle.

In retrospect, ER membrane phase separation has escaped previous observations possibly for three reasons. First, decades of membrane biophysics studies in live cells have been primarily focused on plasma membrane, where high cholesterol level (about 50%) (1) favors L_o and L_d phases instead of solid phase. Second, it has to be observed under nonequilibrium condition, where metabolic activity in the ER perturbs the membrane far enough from equilibrium. Last, the solid-phase membrane is difficult to capture by fluorescent lipid probes due to their poor ER delivery and/or

low partitioning into potentially ordered phase (20). For example, we showed that bulky-labeled BODIPY-C_{12} could not partition in solid domain (Fig. 4). For the same reason, such phase separation could elude the examination of membrane fluidity using fluorescent FA analogs (24), which only report on the liquid phase in ER membrane.

Materials and Methods

Cell Culture and Treatment. HeLa (ATCC) and COS-7 (ATCC) cells were maintained in DMEM (Invitrogen). Labeled or unlabeled fatty acids (Sigma or Cambridge Isotope Lab) were coupled to BSA (Sigma) in 2:1 molar ratio and added to medium to designated concentration. Four hundred micromolar fatty acid was used, if not specified. The ER is visualized in live cells using CellLight ER-GFP (Thermo Fisher Scientific) according to the manufacturer's manual. mCherry-Sec61β was a gift from Gia Voeltz, University of Colorado Boulder, Boulder, CO. Transient transfection was done with Lipofectamine 3000 Reagent (Thermo Fisher Scientific). BODIPY 500/510 C_1, C_{12} (BODIPY-C_{12}) (Molecular Probes) was used as a fluorescent fatty acid tracer at 2 μM. Neutral lipid was stained with 1 μM Nile Red solution (Molecular Probes).

SRS and Fluorescence Imaging and Raman Spectroscopy. The setup for SRS microscopy was similar to what was described earlier (36). Correlative SRS and confocal fluorescence imaging was performed on the same microscope (FV1200; Olympus) and objective (60×, water immersion, N.A. = 1.2, UPlanAPO/IR; Olympus). Spontaneous Raman spectra were acquired using an upright confocal Raman spectrometer (Xplora; HORIBA Jobin Yvon).

1. van Meer G, Voelker DR, Feigenson GW (2008) Membrane lipids: Where they are and how they behave. *Nat Rev Mol Cell Biol* 9:112–124.
2. de Almeida RFM, Fedorov A, Prieto M (2003) Sphingomyelin/phosphatidylcholine/cholesterol phase diagram: Boundaries and composition of lipid rafts. *Biophys J* 85:2406–2416.
3. Simons K, Sampaio JL (2011) Membrane organization and lipid rafts. *Cold Spring Harb Perspect Biol* 3:a004697.
4. Jacobson K, Mouritsen OG, Anderson RGW (2007) Lipid rafts: At a crossroad between cell biology and physics. *Nat Cell Biol* 9:7–14.
5. Omura T, Siekevitz P, Palade GE (1967) Turnover of constituents of the endoplasmic reticulum membranes of rat hepatocytes. *J Biol Chem* 242:2389–2396.
6. Dawidowicz EA (1987) Dynamics of membrane lipid metabolism and turnover. *Annu Rev Biochem* 56:43–61.
7. Borradaile NM, et al. (2006) Disruption of endoplasmic reticulum structure and integrity in lipotoxic cell death. *J Lipid Res* 47:2726–2737.
8. Leamy AK, et al. (2014) Enhanced synthesis of saturated phospholipids is associated with ER stress and lipotoxicity in palmitate treated hepatic cells. *J Lipid Res* 55:1478–1488.
9. Robblee MM, et al. (2016) Saturated fatty acids engage an IRE1α-dependent pathway to activate the NLRP3 inflammasome in myeloid cells. *Cell Rep* 14:2611–2623.
10. Fan J, Sammalkorpi M, Haataja M (2010) Influence of nonequilibrium lipid transport, membrane compartmentalization, and membrane proteins on the lateral organization of the plasma membrane. *Phys Rev E* 81:011908.
11. Lingwood D, Simons K (2010) Lipid rafts as a membrane-organizing principle. *Science* 327:46–50.
12. Holthuis JCM, Menon AK (2014) Lipid landscapes and pipelines in membrane homeostasis. *Nature* 510:48–57.
13. Eggeling C, et al. (2009) Direct observation of the nanoscale dynamics of membrane lipids in a living cell. *Nature* 457:1159–1162.
14. Maxfield FR, Tabas I (2005) Role of cholesterol and lipid organization in disease. *Nature* 438:612–621.
15. Quehenberger O, et al. (2010) Lipidomics reveals a remarkable diversity of lipids in human plasma. *J Lipid Res* 51:3299–3305.
16. Wei L, et al. (2016) Live-cell bioorthogonal chemical imaging: Stimulated Raman scattering microscopy of vibrational probes. *Acc Chem Res* 49:1494–1502.
17. Li L, Wang H, Cheng J-X (2005) Quantitative coherent anti-Stokes Raman scattering imaging of lipid distribution in coexisting domains. *Biophys J* 89:3480–3490.
18. Fu D, et al. (2014) In vivo metabolic fingerprinting of neutral lipids with hyperspectral stimulated Raman scattering microscopy. *J Am Chem Soc* 136:8820–8828.
19. Alfonso-García A, Pfisterer SG, Riezman H, Ikonen E, Potma EO (2016) D38-cholesterol as a Raman active probe for imaging intracellular cholesterol storage. *J Biomed Opt* 21:61003.
20. Klymchenko AS, Kreder R (2014) Fluorescent probes for lipid rafts: From model membranes to living cells. *Chem Biol* 21:97–113.
21. Kuerschner L, et al. (2005) Polyene-lipids: A new tool to image lipids. *Nat Methods* 2:39–45.
22. Karpe F, Dickmann JR, Frayn KN (2011) Fatty acids, obesity, and insulin resistance: Time for a reevaluation. *Diabetes* 60:2441–2449.
23. Listenberger LL, et al. (2003) Triglyceride accumulation protects against fatty acid-induced lipotoxicity. *Proc Natl Acad Sci USA* 100:3077–3082.
24. Hoppa MB, et al. (2009) Chronic palmitate exposure inhibits insulin secretion by dissociation of Ca²⁺ channels from secretory granules. *Cell Metab* 10:455–465.
25. Holzer RG, et al. (2011) Saturated fatty acids induce c-Src clustering within membrane subdomains, leading to JNK activation. *Cell* 147:173–184.
26. Volmer R, van der Ploeg K, Ron D (2013) Membrane lipid saturation activates endoplasmic reticulum unfolded protein response transducers through their transmembrane domains. *Proc Natl Acad Sci USA* 110:4628–4633.
27. Igal RA, Wang P, Coleman RA (1997) Triacsin C blocks de novo synthesis of glycerolipids and cholesterol esters but not recycling of fatty acid into phospholipid: Evidence for functionally separate pools of acyl-CoA. *Biochem J* 324:529–534.
28. Shindou H, Shimizu T (2009) Acyl-CoA:lysophospholipid acyltransferases. *J Biol Chem* 284:1–5.
29. Wang H, et al. (2016) Seipin is required for converting nascent to mature lipid droplets. *Elife* 5:e16582.
30. Radhakrishnan A, Goldstein JL, McDonald JG, Brown MS (2008) Switch-like control of SREBP-2 transport triggered by small changes in ER cholesterol: A delicate balance. *Cell Metab* 8:512–521.
31. Heberle FA, Feigenson GW (2011) Phase separation in lipid membranes. *Cold Spring Harb Perspect Biol* 3:a004630.
32. Volmer R, Ron D (2015) Lipid-dependent regulation of the unfolded protein response. *Curr Opin Cell Biol* 33:67–73.
33. Gaber BP, Yager P, Peticolas WL (1978) Deuterated phospholipids as nonperturbing components for Raman studies of biomembranes. *Biophys J* 22:191–207.
34. Korlach J, Schwille P, Webb WW, Feigenson GW (1999) Characterization of lipid bilayer phases by confocal microscopy and fluorescence correlation spectroscopy. *Proc Natl Acad Sci USA* 96:8461–8466.
35. Chavez JA, Summers SA (2003) Characterizing the effects of saturated fatty acids on insulin signaling and ceramide and diacylglycerol accumulation in 3T3-L1 adipocytes and C2C12 myotubes. *Arch Biochem Biophys* 419:101–109.
36. Shen Y, Xu F, Wei L, Hu F, Min W (2014) Live-cell quantitative imaging of proteome degradation by stimulated Raman scattering. *Angew Chem Int Ed Engl* 53:5596–5599.

CHEMISTRY

BIOPHYSICS AND COMPUTATIONAL BIOLOGY